Journal of Power Sources 196 (2011) 8301–8306

Contents lists available at ScienceDirect

Journal of Power Sources

journal homepage: www.elsevier.com/locate/jpowsour

Tri(ethylene glycol)-substituted trimethylsilane/lithium bis(oxalate)borate electrolyte for $LiMn_2O_4$/graphite system☆

Yuki Kusachi[a], Jian Dong[b], Zhengcheng Zhang[b,*], Khalil Amine[b,**]

[a] EV Energy Development, Nissan Motor Co. LTD, Kanagawa 237-8523, Japan
[b] Chemical Sciences and Engineering Division, Argonne National Laboratory, 9700 South Cass Avenue, Argonne, IL 60439, USA

ARTICLE INFO

Article history:
Received 22 April 2011
Received in revised form 5 June 2011
Accepted 7 June 2011
Available online 15 June 2011

Keywords:
Silane-based electrolyte
Oligo(ethylene glycol) substituted silane
LiBOB
Lithium-ion batteries

ABSTRACT

Silane-based electrolyte is a promising candidate for safer electrochemical energy storage devices because it is thermally and electrochemical stable, less flammable and environmental benign. In this paper, electrochemical properties of one of the silane-based electrolytes, tri(ethylene glycol)-substituted trimethylsilane (1NM3)–lithium bis(oxalate)borate (LiBOB) was studied using $LiMn_2O_4$ as cathode and MAG graphite as anode. When combined with LiBOB as lithium salt, the 1NM3–LiBOB electrolyte can provide solid electrolyte interface (SEI) formation due to the reductive decomposition of LiBOB at first charging cycle. Compared to the electrolyte used in the conventional lithium-ion batteries, 1NM3–LiBOB electrolyte showed compatible battery performance in $LiMn_2O_4$/MAG chemistry. The AC impedance measurement indicates that the activation energy (E_a) obtained from the charge transfer impedance for 1NM3–LiBOB was higher than that of the state-of-the-art electrolyte. Due to its low conductivity, the rate capability of 1NM3–LiBOB electrolyte needs to be improved.

Published by Elsevier B.V.

1. Introduction

Plug-in hybrid electric vehicles (PHEVs) and electric vehicles (EVs) are highly expected to be a major contribution to the energy efficiency of transportation. Lithium ion battery is the most promising candidate as power for electric energy storage device for vehicle application, and EVs using lithium ion battery as power source have been released recently [1]. To deliver EVs to the consumer market, energy storage device should be balanced with high capacity, high power, and long life, low cost and high safety. For vehicle application, due to the huge size of the lithium ion battery pack, high safety is greatly desired compared with the mobile applications such as laptop and mobile phones.

$LiMn_2O_4$ has been commercialized as a cathode active material to achieve safer lithium ion batteries due to its thermally stable characteristics [2,3]. However, these batteries are still using organic carbonates as electrolyte solvents which are flammable and volatile.

Numerous attempts have been made to improve the thermal stability and safety characteristics of the electrolytes in lithium-ion battery for the past two decades [4]. It has been reported that phosphazene-based compounds are investigated as flame retardant additives for organic carbonate electrolytes [5,6]. Recently, ionic liquid is widely explored and reported as a promising candidate for non-flammable electrolytes for lithium and lithium ion battery [7].

Silane-based electrolyte has emerged as a promising candidate for the development of lithium-ion battery in applications such as implantable medical device, electric vehicles (EV), and hybrid electric vehicles (HEV) in which safety is a primary consideration. Comparing to the electrolytes used in the conventional lithium-ion batteries which are flammable, volatile, and highly reactive organic carbonate solvent, silane-based electrolytes are thermally and electrochemical stable, less flammable and environmental benign. The oligo(ethylene glycol)-functionalized silane electrolyte solvents were found to dissolve most lithium salts easily and showed conductivity approaching that of conventional organic carbonate-based electrolyte [8–11]. Tri(ethylene glycol)-substituted trimethylsilane (1NM3, Fig. 1) was identified as a focus of interest due to its well-balanced properties: high conductivity and low viscosity when it was used as a non-aqueous electrolyte [8].

The battery group at Argonne National Laboratory has undertaken tremendous efforts to enable the silane-based electrolyte towards the next generation electrolyte for PHEV/EV applications.

* Corresponding author. Tel.: +1 630 252 7868; fax: +1 630 972 4440.
** Corresponding author. Tel.: +1 630 252 3838; fax: +1 630 972 4672.
E-mail addresses: zzhang@anl.gov (Z. Zhang), amine@anl.gov (K. Amine).

0378-7753/$ – see front matter. Published by Elsevier B.V.
doi:10.1016/j.jpowsour.2011.06.033

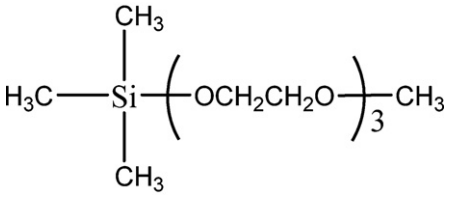

Fig. 1. Molecular structure of tri(ethylene glycol)-substituted trimethylsilane (1NM3).

LiBOB was found to be suitable lithium salt for the silane electrolyte, because it contains no labile fluorine and is thermally stable. It can also provide a passivation film on surface of the graphite anode [12–16]. In 2010, we published our results of silane 1NM3/LiBOB-based electrolyte in $Li(Ni_{1/3}Co_{1/3}Mn_{1/3})O_2$ (NCM) cathode and graphite (MAG) anode lithium ion chemistry [17]. As a continuation of our silane electrolyte, here we report the performance of 1NM3–LiBOB electrolyte in $LiMn_2O_4$ cathode and graphite anode cell chemistry.

2. Experimental

LiBOB (99.87%) and ethylene carbonate (EC)/ethyl methyl carbonate (EMC) were purchased from Novolyte. 1.2 M $LiPF_6$ in 3/7 EC/EMC was purchased from Tomiyama Pure Chemical. All of purchased electrolyte chemicals were used as received. $LiMn_2O_4$ cathode and MAG anode electrodes were provided by EnerDel Inc. The cathode active material loading is 11.5 mg cm^{-2} and balanced with the corresponding anode electrode.

1NM3 solvent was synthesized and analyzed according to our previously reported procedure [17]. ^{1}H, ^{13}C NMR and FT-IR spectroscopy were employed to identify the structure of 1NM3 and its purity. Ionic conductivity measurement was performed using the YSI 3200 Conductivity Instrument equipped with a YSI 3253 conductivity cell.

The charge–discharge cycling performance was evaluated by an Arbin cycler BT-2043. 2032 coin cells were assembled with $LiMn_2O_4$ as the cathode, MAG graphite as the anode, and a microporous polyethylene/polypropylene/polyethylene as the separator. The effective electrode area was 1.6 cm^2. Electrodes were dried in a vacuum oven at 120 °C for overnight before the cell assembling. A two-cycle formation step was applied prior to the cycling test at room temperature by *C*/5 rate. Performance data were acquired and analyzed by the software associated with the instrument.

AC impedance measurements were performed by Auto Lab electrochemical system. The impedance of full cell was measured by applying a sine wave of 10 mV rms over the frequency region of 1 MHz to 10 mHz in an environmental chamber. The impedance measurements were carried out at fully charged state after four-cycle formation process at temperatures from −20 to 60 °C in an environmental chamber. The impedance measurements at different initial charge state were carried out in the environmental chamber at 25 °C. The cell was charged from initial open circuit voltage (OCV) at a rate of *C*/20 for 15 min. After 20 min relaxation, OCV and the impedance were measured, then the cell was charged for another 15 min and measured the OCV and impedance again. This process is repeated until cell voltage reaches 4.2 V. After that, the fully charged cell was stored at room temperature for 2 days, then discharge process was carried out in the same manner using constant current rate *C*/20 for 30 min. This discharge process was repeated until cell voltage reaches 3.0 V. The lithium ion transference number was obtained using the combination of ac impedance and dc polarization method described in Ref. [18] with lithium/electrolyte/lithium symmetry cells.

3. Results and discussion

3.1. Conductivity and transference number (t_{Li^+})

Silane solvent 1NM3 has a high boiling point and a low viscosity [8]. It can easily dissolve most of the lithium salts, such as LiBOB, lithium difluoro(oxalate)borate (LiDfOB), $LiPF_6$, $LiBF_4$, and lithium bis(trifluromethylsulfonyl) imide (LiTFSI) to form the electrolytes. Among these, LiBOB was selected as a lithium salt due to its capability of forming a passivation film on the electrode. In this study, 0.8 M LiBOB 1NM3 (1NM3–LiBOB) was investigated and its performance was compared with1.2 M $LiPF_6$ EC/EMC (3/7) (EC/EMC–$LiPF_6$) as the reference electrolyte.

The ionic conductivities of the 1NM3–LiBOB and EC/EMC–$LiPF_6$ electrolytes as a function of temperature are shown in Table 1. Conductivity of 1NM3–LiBOB is higher than 1 mS cm^{-1} at room temperature, and it is sufficient for the practical application for lithium ion battery. The Li^+ transference number was determined by the method proposed by Evans [19] and refined by Abraham [18], which is combining AC impedance test and DC polarization test on the same Li/Li symmetrical cell. In this test, following equation was used to calculate the lithium transference number:

$$t_{Li^+} = \frac{I_S R_{eS}(\Delta V - I_o R_l^o)}{I_0 R_{eo}(\Delta V - I_S R_l^S)} \quad (1)$$

DC polarization voltage (ΔV) was applied 10 mV for 1 h to obtain the initial current I_0 and stable current I_s The measurement of initial current I_0 is well attuned to the switching noise, measurement time resolution and cell structure. After several test, 100 ms after applying pulse was used as I_0 and 2032 coin cell with 1.2 mm thick separator was used in this study. The bulk resistance, R_e and interfacial resistance, R_l were obtained from the AC impedance before and after dc polarization. A lithium ion transference number (t_{Li^+}) of 0.49 was obtained using this technique for 1NM3–LiBOB electrolyte, which is larger than that for EC/EMC–$LiPF_6$ electrolyte ($t_{Li^+} = 0.20$) and that for EC/EMC–LiBOB electrolyte ($t_{Li^+} = 0.30$). Higher lithium transference number of 1NM3–LiBOB is probably due to smaller size of the solvated lithium cation–silane solvent complex.

3.2. First charge and discharge characteristics

Fig. 2 shows the first charge and discharge profiles of $LiMn_2O_4$/MAG cell charged from OCV to 4.2 V then discharged to 3.0 V with a constant current of *C*/10 at room temperature. In Fig. 2, 1NM3–LiBOB showed a small plateau at early charge stage at around 2.2 V. The cell with 1NM3–LiBOB electrolyte delivered a discharge capacity of 0.85 mAh, which is lower than that for EC/EMC–$LiPF_6$. These characteristics are similar to the electrolyte comprising of carbonates and LiBOB [12]. In $LiMn_2O_4$/MAG cell, the voltage at 2.2 V corresponds to the anode potential at 1.7 V (Li/Li^+) and it is consistent with the reduction potential of LiBOB at anode using carbonate solvents. Therefore even in the silane system, LiBOB decomposed at first charge process at 1.7 V (Li/Li^+) forming a solid electrolyte interphase on the graphite anode. The detailed characterization of this SEI layer formed by LiBOB in 1NM3–LiBOB electrolyte system will be reported in a separate paper shortly.

3.3. Cycling performance of 1NM3–LiBOB

Fig. 3 shows the cycling performance of $LiMn_2O_4$/MAG with 1NM3–LiBOB electrolyte. After the formation cycles, the cells were repeatedly charged and discharged with a current of *C*/5 rate between 3.0 and 4.2 V. Discharge capacity was normalized by the 2nd cycle discharge capacity. Fig. 3(a) is the room temperature

Table 1
Conductivities and lithium ion transference number for 1NM3 electrolyte and EC/EMC electrolyte.

Electrolyte	σ at −20 °C mS cm^{-1}	σ at 25 °C mS cm^{-1}	σ at 50 °C mS cm^{-1}	t_{Li^+}
0.8 M LiBOB–1NM3	0.46	1.7	2.2	0.49
1.2 M $LiPF_6$–EC/EMC	2.2	8.1	12	0.20
0.8 M LiBOB–EC/EMC	–	–	–	0.30

cycling performance. It clearly shows that 1NM3–LiBOB electrolyte has comparable property with the conventional EC/EMC–$LiPF_6$ electrolyte.

It was reported that $LiMn_2O_4$ suffers from the serious capacity fading in the lithium-ion cells due to Mn^{2+} dissolution in $LiPF_6$-based conventional electrolyte especially at high temperature [20]. To overcome this issue, LiBOB as lithium salt was investigated in carbonate electrolytes [3]. Silane electrolyte using LiBOB as salt may provide advantages over the conventional electrolyte due to its low polarity. Fig. 3(b) illustrates the cycling performance at 55 °C of the cell with EC/EMC–$LiPF_6$ showed significant capacity decay (54% capacity loss) at 60 cycles, while the cell using 1NM3–LiBOB still maintained high capacity retention (60% of the initial discharge capacity) at the same cycle number. The improved cell performance using 1NM3–LiBOB electrolyte is considered to be the lower solubility of the high oxidation sate of Mn ions in 1NM3–LiBOB and absence of the HF generated by $LiPF_6$ with trace moisture in the conventional $LiPF_6$-based electrolyte. From this test, it is demonstrated that 1NM3 solvent is acceptable in $LiMn_2O_4$/MAG cell with LiBOB as a salt even at elevated temperature. However, the cell with 1NM3–LiBOB electrolyte showed fast capacity fade after 60 cycles at 55 °C. This phenomenon is not yet well understood.

3.4. Rate capability

The rate capabilities of 1NM3–LiBOB electrolyte were evaluated by charging a $LiMn_2O_4$/MAG cell with a constant current equivalent to *C*/10 to 4.2 V, followed by a constant voltage charge until the cutoff current equivalent to *C*/20. The cell was then discharged to 3.0 V at constant currents of *C*/5, *C*/2, 1*C*, 2*C* and 3*C*. As shown in Fig. 4(a), the $LiMn_2O_4$/MAG cell using EC/EMC–$LiPF_6$ as the electrolyte can deliver more than 90% capacity retention at the *C*/2, 1*C*, 2*C* and 3*C* rates. The $LiMn_2O_4$/MAG cell using 1NM3–LiBOB as the electrolyte (Fig. 4(b)) showed more than 90% and 70% capacity retention at the *C*/2 and 1*C* rates, respectively. However, when discharged at the 2*C* rate, the 1NM3–LiBOB electrolyte cell only showed less than 40% capacity. The resistance calculated from the voltage drop within 1 s after the discharge showed 21 Ω and 149 Ω for EC/EMC–$LiPF_6$ and 1NM3–LiBOB, respectively. The severe capacity fading of 1NM3–LiBOB at high rate should be attributed to the lower conductivity of electrolyte and the resistive SEI formed by the decomposition of LiBOB on the graphite anode surface [21–23].

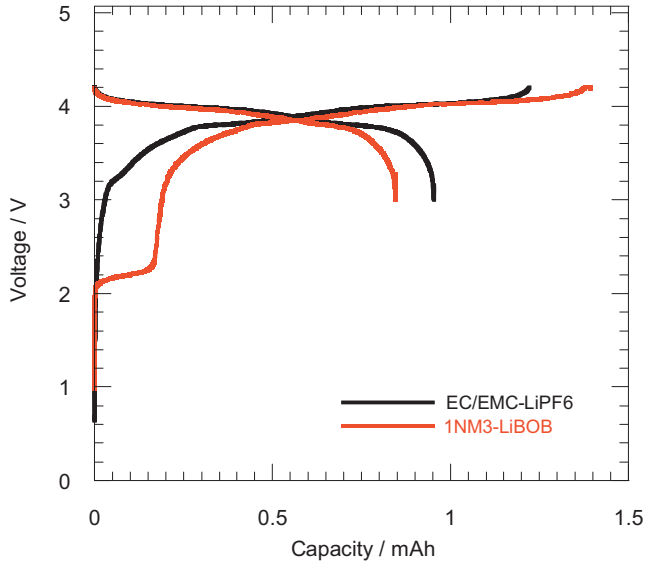

Fig. 2. First charge–discharge profile of graphite/$LiMn_2O_4$ cell using 0.8 M LiBOB in 1NM3 and 1.2 M LiPF6 in EC/EMC 3/7.

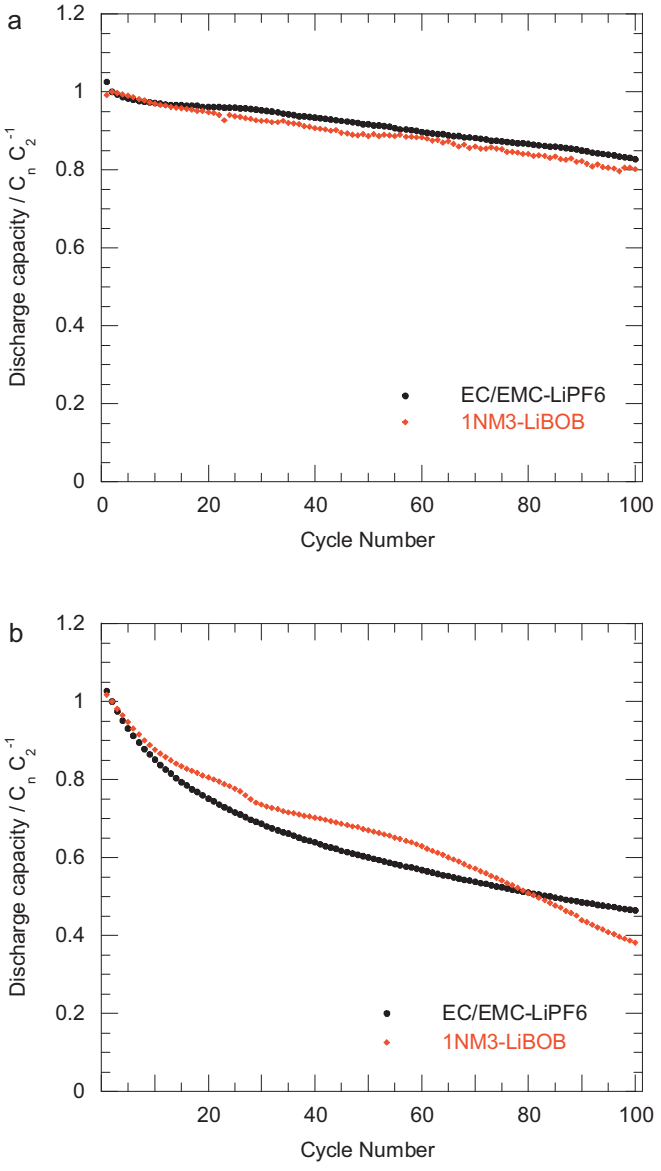

Fig. 3. Cycling performance of graphite/$LiMn_2O_4$ cell using 0.8 M LiBOB in 1NM3 and 1.2 M LiPF6 in EC/EMC 3/7: (a) 25 °C and (b) 55 °C.

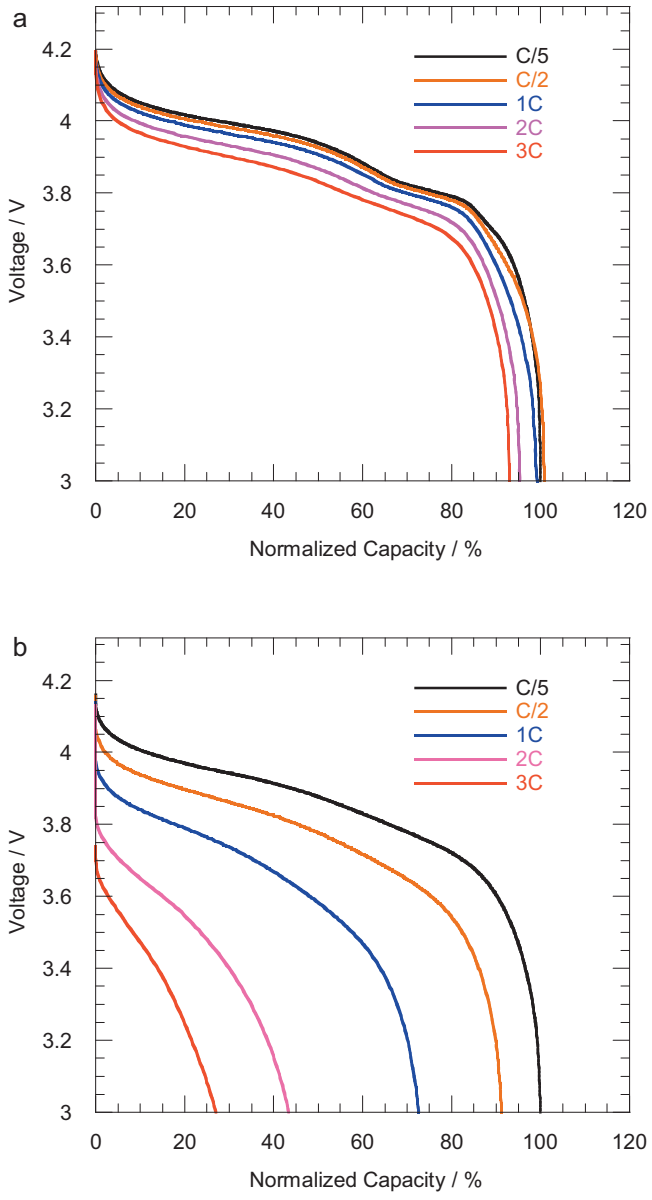

Fig. 4. Discharge rate capability of graphite/$LiMn_2O_4$ cell with *C*/5, *C*/2, 1*C*, 2*C* and 3*C* rate: (a) 1.2 M LiPF6 in EC/EMC 3/7 and (b) 0.8 M LiBOB in 1NM3.

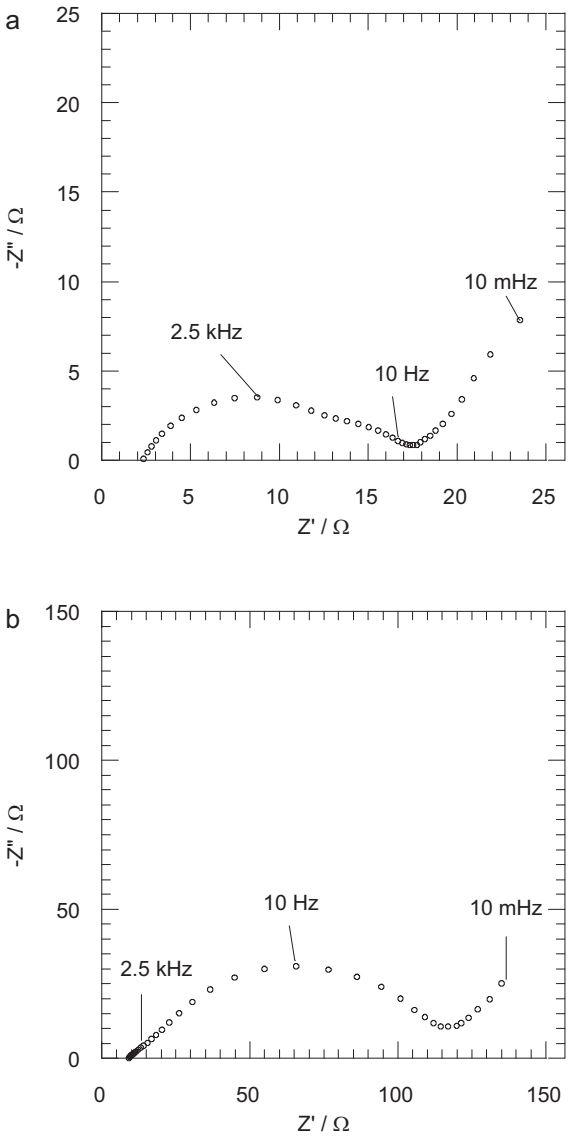

Fig. 5. Nyquist plots of graphite/$LiMn_2O_4$ cells at 30 °C: (a) 1.2 M LiPF6 in EC/EMC 3/7 and (b) 0.8 M LiBOB in 1NM3.

3.5. Electrochemical impedance spectroscopy of 1NM3–LiBOB

The ac impedance measurements of $LiMn_2O_4$/MAG cell using EC/EMC–$LiPF_6$ electrolyte and 1NM3–LiBOB electrolyte were measured at 4.2 V fully charge state (Fig. 5). Two cells using different electrolytes showed two semicircles on Nyquist plots. The semicircle in the middle frequency (1 kHz to 1 Hz) showed significant difference where the cell using 1NM3–LiBOB electrolyte showed larger impedance. It has been widely accepted that middle frequency region is assigned to interfacial film on the electrode, and low frequency region is assigned to charge transfer and solvation–desolvation process [24–26]. However, these data need to be assigned carefully due to the complex of impedances with cathode–electrolyte interface and anode–electrolyte interface, impedance data were fitted to a common equivalent circuit model as shown in Fig. 6. The middle frequency region semicircle resistance was assigned to R_1 and low frequency region semicircle resistance was assigned to R_2. Fig. 7 summarizes the extracted parameters from the ac impedance results measured at temperatures from −20 to 60 °C. For simplicity, if one R value is 10 times larger than another R, the smaller R was neglected due to the large fitting error. At middle frequency semicircle, resistance R_1 using EC/EMC–$LiPF_6$ was independent with temperature. In contrast, R_1 using 1NM3–LiBOB showed large temperature dependence and it follows Arrhenius relation with activation energy E_a of 32.4 kJ mol^{-1}. At low frequency semicircle, R_2 for 1NM3–LiBOB cell showed 25–50 times larger than that using EC/EMC–$LiPF_6$ in the measurement temperature range. This huge resistance of R_2 for 1NM3–LiBOB electrolyte may be due to the thick SEI formed by LiBOB decomposition. Activation energies of 63.9 kJ mol^{-1} and 77.9 kJ mol^{-1} were obtained for EC/EMC–$LiPF_6$ and 1NM3–LiBOB,

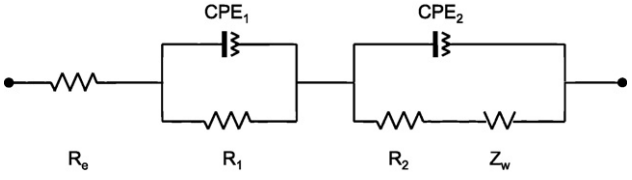

Fig. 6. Circuit model of battery impedance adapted to parameter fitting.

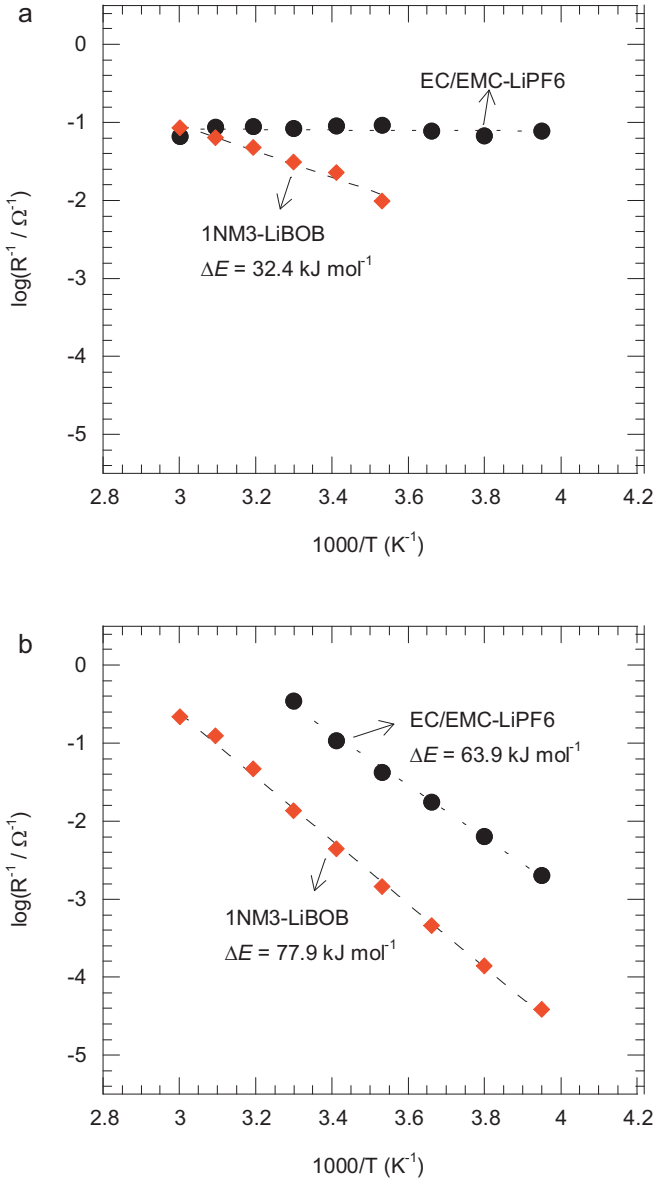

Fig. 7. Cell ac impedance–temperature dependence at fully charged state: (a) R_1 corresponding to middle frequency range semicircle and (b) R_2 corresponding to low frequency range semicircle. Activation energy was obtained from the slope.

respectively. Typical activation energy of charge transfer resistance was reported in the range of 50–70 kJ mol^{-1} [24–26]. The activation energy value achieved for EC/EMC–LiPF$_6$ in our test falls in this range. Therefore, it is rational to assign R_2 as charge transfer impedance. However, for 1NM3–LiBOB system, it showed much larger E_a than the typical value. This large E_a could be related to the strong coordination of Li^+ with oligo(ethylene glycol) group in 1NM3 molecular structure.

3.6. Impedance analysis of 1NM3–LiBOB during first cycle

As described above, $LiMn_2O_4$/MAG cell using 1NM3–LiBOB electrolyte showed larger charging capacity, irreversible capacity and impedance. To further understand the property of 1NM3–LiBOB electrolyte, ac impedances were measured during the first charge–discharge cycle. The cell was charged from initial open circuit voltage (OCV) at a rate of $C/20$ for 15 min. After 20 min relaxation, the impedance was measured, then the cell was charged for another 15 min and measured the impedance again.

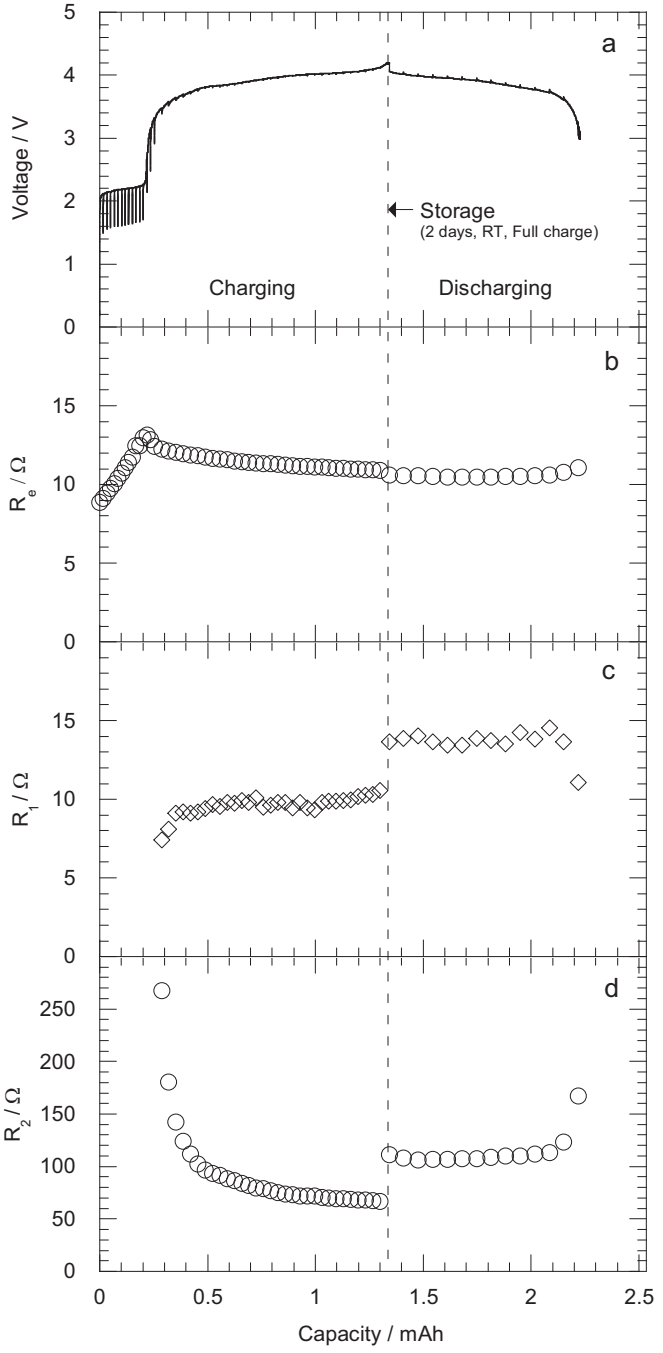

Fig. 8. Cell impedance–charge state dependence of the graphite/0.8 M LiBOB in 1NM3/$LiMn_2O_4$ for the first cycle: (a) charge and discharge profiles of the cell with current interruptions, (b) Ohmic resistance R_e, (c) resistance corresponding to middle frequency range semicircle R_1, and (d) resistance corresponding to low frequency range semicircle R_2.

This process is repeated until cell voltage reaches 4.2 V. After that, the fully charged cell was stored at room temperature for 2 days, then discharge process was carried out in the same manner using constant current rate $C/20$ for every 30 min until the cell voltage reaches 3.0 V. As shown in Fig. 8(a), large over potential was observed during the charging plateau starting at 2 V due to LiBOB decomposition reaction. In order to extract resistance parameter, AC impedance data during first cycle was adapted to model circuit shown in Fig. 6. The ohmic resistance, R_e was extracted from x-axis intercept on Nyquist plot. Then other parameters were extracted from the curve fitting. Fig. 8(b)–(d) shows resistance variation dur-

ing the first cycle. It is clear that the ohmic resistance R_e was linearly increased with LiBOB decomposition extent at 2.2 V. R_e reached maximum value of 13.1 Ω which is 50% larger than the initial resistance (Fig. 8(b)). In our previous paper [17], we have reported the cell with 0.8 M LiBOB in 1NM3 electrolyte shows less capacity and cycling stability than that of 1.2 M LiBOB in 1NM3 electrolyte, which is inconsistent with their room temperature ionic conductivities since higher conductivity electrolyte facilitates ion transport during the charge–discharge cycle in lithium-ion battery. Both results indicate that LiBOB decomposition during the 1st charge process will lead to the reduction of LiBOB concentration. As a result, the 1NM3–LiBOB electrolyte was not able to maintain sufficient salt concentration after the formation of the passivation film during the first cycle. Compared with R_e at 2.2 V plateau, ohmic resistance R_e gradually became smaller. We ascribed this phenomenon to the excess electrolyte inside dead volume of coin cell. The excess electrolyte will diffuse to the active electrode pores, resulting to the ohmic resistance decrease. In contrast, after LiBOB decomposition, the middle frequency range resistance R_1 showed relatively stable and low frequency range resistance R_2 decreased and stabilized gradually. This suggests the LiBOB decomposition at 2.2 V plays an important role for the interfacial impedance during first charging. The subsequent electrochemical process does not affect too much on the electrode/electrolyte interfacial impedance. However, when stored at fully charged state for 2 days at room temperature, both R_1 and R_2 showed significant increase as shown from Fig. 8 (c for R_1, d for R_2), indicating that LiBOB continually decomposes forming a thick SEI at fully charged state after primary SEI formation during first charge.

To address this issue, extensive investigations employing $LiPF_6$, the state-of-the-art lithium salt, with 1NM3 solvent are in progress and will be reported in a separate paper.

4. Conclusions

The tri(ethylene glycol)-substituted trimethylsilane (1NM3)–LiBOB was evaluated as electrolyte for $LiMn_2O_4$ cathode and MAG graphite anode system. This new electrolyte can enable the lithium ion cell performance after first formation cycle due to the SEI formation by LiBOB decomposition on the surface of electrode. Excellent cycling performance was achieved both at room temperature and at 55 °C which is comparable with the state-of-the-art electrolyte. However, due to the less conductive 1NM3–LiBOB electrolyte and resistive SEI, the rate capability was not as good as that for conventional EC/EMC–$LiPF_6$ electrolyte. Electrochemical impedance studies were carried out to understand interfacial phenomena. It was found that activation energy obtained from charge transfer impedance was higher than that of EC/EMC–$LiPF_6$. It could be noted that 1NM3 solvent has slower kinetics due to the strong coordination with Li^+. More impedance measurements during first charging process revealed SEI formation by LiBOB decomposition leading to the decrease of the electrolyte conductivity. Our results in this study suggest that 1NM3 is an appropriate solvent for lithium ion battery and other electrochemical systems.

Acknowledgement

This research is supported by EnerDel Inc and Nissan Motor Co., LTD.

References

[1] Nissan Motor Co., Ltd., http://www.nissan-global.com/EN/NEWS/2009/_STORY/090802-02-e.html (Last visited: 2011.4.15).
[2] Y. Xia, M. Yoshio, in: G.-A. Nazri, G. Pistoia (Eds.), Lithium Batteries, Springer, US, 2003, p. 361.
[3] K. Amine, J. Liu, S. Kang, I. Belharouak, Y. Hyung, D. Vissers, G. Henriksen, J. Power Sources 129 (2004) 14.
[4] K. Xu, Chem. Rev. 104 (2004) 4303.
[5] D.H. Doughty, E.P. Roth, C.C. Crafts, G. Nagasubramanian, G. Henriksen, K. Amine, J. Power Sources 146 (2005) 116.
[6] M. Otsuki, T. Ogino, in: M. Yoshio, R.J. Brodd, A. Kozawa (Eds.), Lithium-Ion Batteries, Springer, New York, 2009, p. 275.
[7] H. Sakaebe, H. Matsumoto, Electrochem. Commun. 5 (2003) 594.
[8] K. Amine, Q.Z. Wang, D.R. Vissers, Z.C. Zhang, N.A.A. Rossi, R. West, Electrochem. Commun. 8 (2006) 429.
[9] H. Nakahara, S. Nutt, J. Power Sources 158 (2006) 1386.
[10] Z.H. Chen, H.H. Wang, D.R. Vissers, L.Z. Zhang, R. West, L.J. Lyons, K. Amine, J. Phys. Chem. C 112 (2008) 2210.
[11] L.Z. Zhang, Z.C. Zhang, S. Harring, M. Straughan, R. Butorac, Z.H. Chen, L. Lyons, K. Amine, R. West, J. Mater. Chem. 18 (2008) 3713.
[12] K. Xu, S.S. Zhang, T.R. Jow, W. Xu, C.A. Angell, Electrochem. Solid-State Lett. 5 (2002) A26.
[13] T.R. Jow, K. Xu, M.S. Ding, S.S. Zhang, J.L. Allen, K. Amine, J. Electrochem. Soc. 151 (2004) A1702.
[14] K. Xu, U. Lee, S.S. Zhang, T.R. Jow, J. Electrochem. Soc. 151 (2004) A2106.
[15] K. Xu, J. Electrochem. Soc. 155 (2008) A733.
[16] L. Larush-Asraf, M. Biton, H. Teller, E. Zinigrad, D. Aurbach, J. Power Sources 174 (2007) 400.
[17] J. Dong, Z. Zhang, Y. Kusachi, K. Amine, J. Power Sources 196 (2011) 2255.
[18] K.M. Abraham, Z. Jiang, B. Carroll, Chem. Mater. 9 (1997) 1978.
[19] J. Evans, C.A. Vincent, P.G. Bruce, Polymer 28 (1987) 2324.
[20] Y.Y. Xia, Y.H. Zhou, M. Yoshio, J. Electrochem. Soc. 144 (1997) 2593.
[21] Z.C. Zhang, J.A. Dong, R. West, K. Amine, J. Power Sources 195 (2010) 6062.
[22] Z.H. Chen, Y. Qin, J. Liu, K. Amine, Electrochem. Solid-State Lett. 12 (2009) A69.
[23] Z.H. Chen, W.Q. Lu, J. Liu, K. Amine, Electrochim. Acta 51 (2006) 3322.
[24] T. Abe, H. Fukuda, Y. Iriyama, Z. Ogumi, J. Electrochem. Soc. 151 (2004) A1120.
[25] T. Abe, F. Sagane, M. Ohtsuka, Y. Iriyama, Z. Ogumi, J. Electrochem. Soc. 152 (2005) A2151.
[26] K. Xu, J. Electrochem. Soc. 154 (2007) A162.